Am J Cancer Res 2022;12(3):1027-1041
www.ajcr.us /ISSN:2156-6976/ajcr0141828

Original Article

Targeted delivery of a PROTAC induced PDEδ degrader by a biomimetic drug delivery system for enhanced cytotoxicity against pancreatic cancer cells

Ruyu Fan[1*], Shipeng He[2*], Yongqing Wang[1*], Jiaming Qiao[1], Hongcheng Liu[3], Levon Galstyan[1,4], Arman Ghazaryan[1,4], Hui Cai[1], Shini Feng[1], Pinyue Ni[1], Guoqiang Dong[5], Huafei Li[1]

[1]School of Lifesciences, Shanghai University, 333 Nanchen Road, Shanghai 200444, China; [2]Institute of Translational Medicine, Shanghai University, 333 Nanchen Road, Shanghai 200444, China; [3]Department of Thoracic Surgery, Shanghai Pulmonary Hospital Affiliated to Tongji University, Shanghai 200433, China; [4]SLAVMED Medical Center, Manandyan Street, 9 Bld., Yerevan, R.A., Armenia; [5]Department of Medicinal Chemistry, School of Pharmacy, Second Military Medical University, 325 Guohe Road, Shanghai 200433, China. [*]Equal contributors.

Received January 18, 2022; Accepted February 27, 2022; Epub March 15, 2022; Published March 30, 2022

Abstract: Pancreatic carcinoma (PC) has one of the highest mortality-to-incidence ratios of any solid tumor worldwide. Although KRAS mutation is commonly found in 95% of PCs, directly targeting KRAS remains to be a highly challenging task because of its lacking catalytic pockets where molecule inhibitors can bind with. Proteolysis-targeting chimeric (PROTAC) represents an effective approach for specific degradation of disease-causing proteins by hijacking the endogenous ubiquitin-proteasome system (UPS). Previously, we designed a first-in-class PROTAC induced PDEδ degrader (PIPD), which demonstrated improved anti-tumor efficacy against KRAS mutant malignancies. However, translating cellular degradative effects from bench to beside remains a highly challenging task because of PROTAC's poor penetration efficiency across target cytomembranes and non-targeting delivery induced undesired "off target" side-effects. Herein, a smart nano-drug delivery system (CM8988-PIPD) was successfully constructed by biomimetic strategy for targeted delivery of PIPD. The biomimetic nanoparticle showed well-defined regular spherical structure with an average particle size of approximately 124.8 nm. Cancer cytomembrane camouflage endows CM8988-PIPD with excellent *in vivo* serum stability, controlled drug release profile, favorable biocompatibility & immunocompatibility, and prominent targeting ability to homologous PC cells. Owing to these advantages, the smart DDS significantly enhanced PDEδ degrading efficacy, resulting in induced cellular apoptosis (more than 50% for both PC cells) and suppressed cell proliferation via the inhibition of RAS signaling. *In vitro* studies illustrated that CM8988-PIPD hold great potential for the treatment of PC, which merits further investigation in both pre-clinical and clinical investigations in the future.

Keywords: Pancreatic carcinoma, KRAS mutation, proteolysis-targeting chimeric, biomimetic drug delivery system, PDEδ

Introduction

Pancreatic carcinoma (PC) is a highly fatal disease with a 5-year survival of 3-15% worldwide, which has one of the highest mortality-to-incidence ratios of any solid tumor and is becoming an increasingly common cause of cancer mortality [1, 2]. According to the statistics of the American Cancer Society (ACS), the numbers of new pancreatic cancer cases and deaths were estimated to be respectively 62,210 and 49,830 in 2022 in the United States nationally [3]. Surgical resection represents the only chance for cure, and the prognosis is also substantially better for patients diagnosed at an operable rather than an inoperable stage [4]. Unfortunately, more than 85% patients have cancers that are not surgically resectable at the time of diagnosis owing to no obvious specific symptoms in the early stage of disease [5]. Therefore, finding safe and effective methods for treating PC is urgently needed.

Past decades witness the emerging development of many innovative therapeutic strategies

towards malignancies, by silencing the complementary mRNA with RNA interfering (RNAi) or microRNA (miRNA), or blocking/activating the biological function of protein targets with either small molecules (inhibitors/agonist) or monoclonal antibodies (mAbs), or stimulating the immune system to destroy tumors, or correcting the DNA mutations with gene editing techniques (such as CRIPSR technology) [6-8]. Currently, more than 50 small molecule inhibitors (SMIs) have been approved by the Food and Drug Administration (FDA) for the treatment of cancer [6]. Those SMIs are largely developed by large-scale screening and optimized to achieve a desired binding with the well-defined active sites of each target protein, thereby inhibiting its biological activity [9, 10]. However, a variety of proteins other than kinase have no definite active sites and have been termed as non-druggable targets for a long time, among which RAS is a typical example [6, 11].

RAS family proteins are a kind of small guanosine triphosphate (GTPase) connecting cell membrane growth factor receptors to intracellular signaling transducers and transcription factors, thus playing vital roles in cell proliferation, differentiation and apoptosis, etc. [12, 13]. Mutational activation of RAS is a universal feature accounting for ~30% of malignancies, with Kirsten RAS (KRAS) being the most frequently mutated isoform [14, 15]. KRAS mutation is commonly found in 95% of PCs, which is well recognized as an ideal target candidate [15, 16]. However, direct targeting KRAS by SMIs remains to be a highly challenging task owing to its nearly spherical structure lacking suitable catalytic pockets where SMIs are designed to bind with [17].

KRAS proteins can be activated by binding to GTP only after being effectively attached to the cytomembrane [17]. During its way to the cytomembrane, KRAS binds to a shuttling factor called PDEδ through its farnesylated hypervariable region, preventing KRAS's binding to endomembranes and facilitating its diffusion throughout the cell [18, 19]. On the basis of its pivotal roles, we designed a first-in-class PDEδ degrader by proteolysis-targeting chimeric (PROTAC) technology in our previous study [20]. The promising PROTAC induced PDEδ degrader (termed as PIPD for short hereafter) can efficiently induce PDEδ degradation and demonstrates significantly improved anti-tumor efficacy against KRAS mutant SW480 cells [20].

PROTAC is a new strategy firstly emerged in 2001, which represents an effective approach for specific degradation of disease-causing proteins by hijacking the endogenous ubiquitin-proteasome system (UPS) [21]. Generally, PROTAC molecules are ternary chemical complexes consisting of three functional parts: (1) a ligand for recruiting an E3 ubiquitin ligase; (2) a ligand that binds a target protein; (3) a linker that connects these two active ingredients [9, 22]. Upon this smartly designed formation, PROTAC molecules can form ternary complex together with E3 ligase and POI, mediating the transferring of ubiquitin tags onto the POI by hijacking E3 ligase [23]. Appropriately ubiquitin-tagged POIs are then recognized by the 26S proteasome and proteolytically cleaved (**Figure 1**) [23].

Although PROTAC has been successfully employed for degrading a variety of cancer promoting proteins in laboratory investigation, translating cellular degradative effects from bench to beside remains a highly challenging task [23]. To date, only two PROTAC degraders against ER (ARV-471) and AR (ARV-110) have been progressed into clinical trials for patients with either $ER^+/HER2^-$ locally advanced/metastatic breast cancer, or metastatic castration resistant prostate cancer in 2019 [9, 24]. Some potential shortages of PROTAC may limit its clinical transformation. The larger size of PROTACS (molecular weight >1000 Da) relative to traditional small molecule agents may result in poorer penetration efficiency across target cytomembranes [25]. Because ubiquitin ligases are expressed widely across cell types, PROTAC-induced degradation has been observed in both healthy and diseased tissues suggestive of undesired "off target" side-effects [24, 25]. Besides, the intrinsic pharmacokinetic profile needs to be suitable to allow sufficient drug exposure for long enough to achieve protein knockdown [25, 26].

In the past decades, a variety of smart nano-sized drug delivery systems (DDSs) were designed and developed for enhancing the local content and cellular uptake of therapeutic agents [27, 28]. The biomimetic strategy with

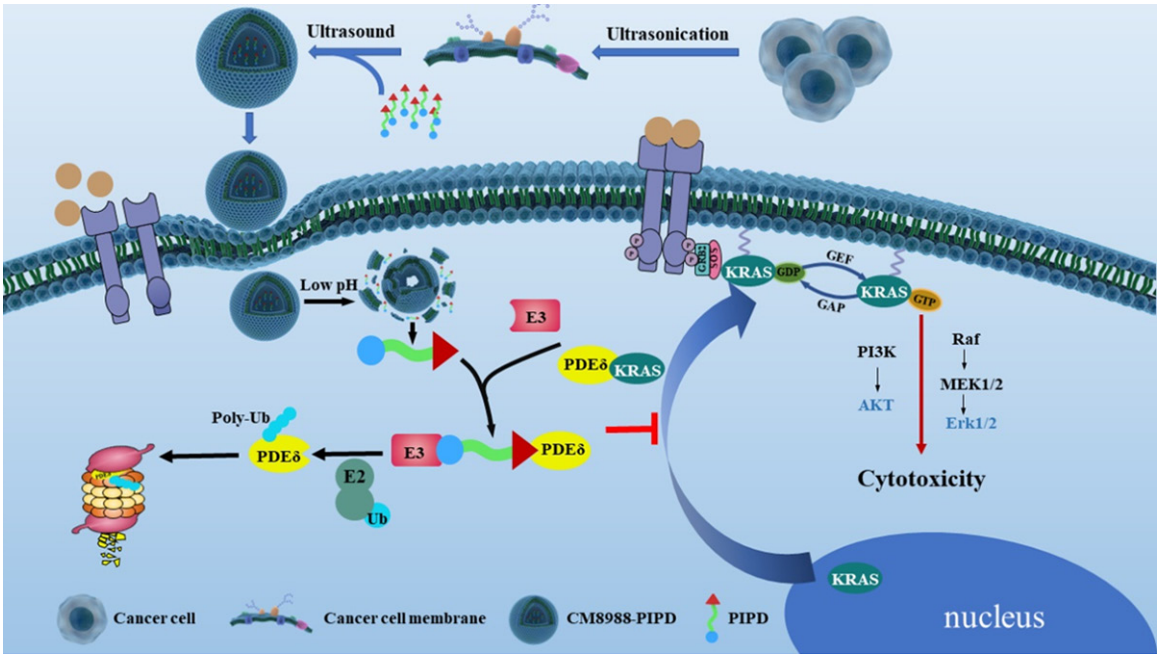

Figure 1. Schematic illustration of homotypic cell membrane-cloaked biomimetic nanocarrier for targeted delivery of PIPD and its anti-tumor mechanism against PC cells. Enhanced anti-cancer efficacy can be attributed to the synergistic effects of (1) targeted delivery of encapsulated PIPD molecules to tumor tissues by favorable serum stability, biocompatibility and immunocompatibility; (2) elevated tumor uptake of bionic nanosized DDS via homologous cell membrane recognition; (3) inhibition of KRAS signal transduction pathway by efficient PDEδ degradation through hijacking the UPS system by released PIPD molecules in target cells.

utilization of natural cell membrane camouflage is one of the most promising technologies for drug delivery which has been extensively employed for diagnosing and treating malignancies [27, 29]. Biomimetic nanoparticles (NPs) integrate the functionality of biological materials with the flexibility of synthetic materials to achieve effective navigation and interfacing in complex biological systems. Except for the enhanced permeability and retention (EPR) effect, adhesion molecules expressed on cytomembrane vectors can navigate and anchor cancer cells through receptor-ligand binding, promoting the drug accumulation of encapsulated agents in diseased tissues and cells [27, 30, 31]. In addition, cytomembrane coating provides a novel biomimetic platform that can mimic the function of source cells when interacting with surrounding biological components [32]. Acquiring the repertoire of surface proteins from source cells, cancerous membrane coated NPs, which own favorable biocompatibility, low toxicity, and good biodegradability, can effectively avoid the scavenging effect of immune system, resulting in enhanced anti-phagocytic ability and prolonged circulation time *in vivo* [32-34]. Besides, membrane camouflage makes them potentially useful as decoys to interfere interactions between cancerous and cancer stromal cells, which mediate many of the aggressive characteristics of cancer [34, 35].

Inspired by these superiorities, a novel biomimetic nano-drug delivery system was successfully designed for targeted delivery of PIPD to pancreatic cancer cells to circumvent the limitations of PROTAC in this study. Our experimental results demonstrate that applying homotypic cancer cell membrane as a cloak to generate desirable DDS could endow nanocarrier with excellent homotypic targeting ability and favorable biocompatibility & immunocompatibility, resulting in prominent tumor suppressing activity against pancreatic cancer *in vitro* (**Figure 1**).

Materials and methods

Materials and cells

Two human PC cell lines (PATU-8988 and PL-45), human liver cancer cell line (SMMC-

7721) and mouse mononuclear macrophage cells (J774A.1) were all obtained from the American Type Culture Collection (ATCC, Manassas, VA, USA). Cells were incubated in Dulbecco's modified eagle medium (DMEM) containing 10% (v/v) fetal bovine serum (FBS, Gibco, Massachusetts, U.S.A.) and 1% penicillin/streptomycin (Thermo Fisher Scientific, Massachusetts, U.S.A.) in a humidified incubator at 37°C with 5% CO_2. The PROTAC compound PIPD was synthesized as described in our previous publication [20]. Alexa Fluor® 488 Annexin V/Dead Cell Apoptosis Kit and LIVE/DEAD™ Fixable Dead Cell Stain Kit were purchased from Thermo Fisher Scientific (Massachusetts, U.S.A.). Protease-inhibitor PMSF, DAPI nuclear staining solution, 4% paraformaldehyde fixation solution, and Coomassie brilliant blue were purchased from Beyotime Biotechnology (Shanghai, China).

Cell membrane extraction

Cancer cytomembrane was extracted according to the previously reported methods with minor changes [36]. In brief, cells were collected, washed with pre-cooled PBS, lysed with lysis buffer containing protease-inhibitor PMSF at 4°C for 12 h, sonicated at 80W-100W for 10 m, and then centrifuged at 20,000 g for 20 m. The supernatant was collected and centrifuged (100,000 g × 30 m), the precipitate was then collected, resuspended in PBS and stored at -80°C for future use.

Encapsulation of PIPDs into biomimetic DDS

PIPD and extracted cytomembrane were mixed and subjected to ultrasonic oscillation (5 min, 28 kHz, 35 W) on ice. The solution was dialyzed against PBS with a membrane (molecular weight cut-off: 3 kDa) at 4°C overnight to remove unencapsulated PIPD molecules. PIPDs encapsulated within the cytomembrane of PATU-8988 and SMMC-7721 cells were respectively marked as CM8988-PIPD and CM7721-PIPD. The concentration of PIPD in the dialysis solution outside the dialysis bag was determined by UV-vis spectrophotometry (absorption at 254 nm) using a standard curve method and recorded as C_{out}. The exact quantity of PIPD in the biomimetic DDS was determined as W_{total}-C_{out}×V_{out}, where W_{total} and V_{out} respectively represents the total PIPD added for encapsulation and the total volume of dialysis solution outside the dialysis bag). The encapsulation efficiency (EE) of PIPD was calculated according to the following function: $EE(\%) = \frac{W_{total} - C_{out} \times V_{out}}{W_{total}} \times 100\%$. In order for fluorescence labelling, the quantum dots (QDs) were encapsulated into the biomimetic DDS in the same way.

Cell membrane integrity analysis

The membrane protein characterization was conducted by SDS-PAGE as previously described [37]. Briefly, samples were prepared with 1 mg/mL final protein concentration in the loading buffer and heated in a metal bath for 10 min. Samples were subjected to SDS-PAGE, and protein bands were stained by using Coomassie blue before imaging.

Characterization of PIPD encapsulated biomimetic DDS

The ζ-potential, hydrodynamic diameter and size distribution of prepared samples were performed by ZetaSizer (Nano-ZS, Malvern Instruments, UK) equipped with a HeeNe laser (633 nm) at the scattering angle 173°. Transmission electron microscopy (TEM, Emesis Veleta G3 transmission electron microscope) was employed to observe the morphology of biomimetic DDS. For preparing the specimens for TEM, the droplet containing biomimetic nanoparticles was placed on Holey Carbon Coated-Copper 200 mesh Grids (Ted Pella, California, USA). Samples were examined on TEM at 80 kV after air-dried. Structure and spectral characteristics of NPs were measured by X-ray photoelectron spectroscopy (XPS, K-alpha, Thermo Scientific, USA) and Fourier transform infrared spectrometer (FTIR, Nicolet AVATAR 370, Thermo Scientific, USA), respectively. UV/Vis spectroscopy was employed to detect the absorbance of free and encapsulated PIPD, respectively.

Serum stability evaluation

For evaluating the serum stability of biomimetic DDS, DMEM supplemented with 50% (v/v) FBS was employed as an *in vitro* serum model to mimic the *in vivo* status. Then CM8988-PIPD was mixed with the resulting serum model at 37°C for 6 d. DLS was employed to measure the size distribution profile every day.

In vitro drug release

A dialysis bag (molecular weight cut-off: 3.5 kDa) containing 2 mL CM8988-PIPD solution was put in a beaker containing 10 mL of PBS, which was fixed in a water bath to keep the temperature at 37°C with continuous stirring. At various time points, 500 μL samples outside the dialysis bag were taken up and the concentration of PIPD was measured by UV/Vis spectroscopy (absorption at 254 nm) using a standard curve method. Cumulative release of PIPD was calculated by the following function:

$$\text{Cumulative release} = \frac{C_{Outside} \times 10\ ml}{C_{Inside} \times 2.0\ ml} \times 100\%$$

Biocompatibility

Different concentrations of free and CM8988 encapsulated PIPDs were added to the suspended red blood cells isolated from mouse orbital blood and kept in room temperature (RT). Mili-Q water and PBS buffer was respectively employed as the positive and negative control. After a 3-hour-incubation, cells were centrifuged (10,000 g × 5 m), the supernatant was then collected and added to a 96-well plate. The absorbance (Ab) of the supernatant at 540 nm was measured and the hemolysis rate was calculated according to the following function:

$$\text{Hemolysis rate (\%)} = \frac{Ab_{drug} - Ab_{negative}}{Ab_{positive} - Ab_{negative}} \times 100\%$$

Cellular uptake

Cellular uptake of the biomimetic NPs was observed by confocal laser scanning microscopy (CLSM) and quantitatively analyzed by flow cytometry (FCM). For CLSM, cells were seeded in special culture dishes at a density of 3×10^4/well for 12 h. Equal concentration of free and encapsulated QDs were then added and co-cultured for another 2 h. The cells were fixed with 4% paraformaldehyde, stained with DAPI for 5 m protecting from light at RT. After then, cells were washed and subjected to confocal microscopic observation. For FCM, cells were inoculated in 6-well plates at a density of 2×10^5/well. After 24 h of culture, equal amount of free and encapsulated QDs were added and co-cultured for another 2 h. Then, cells were collected, washed, and the fluorescence intensity of QDs was analyzed by a Flow Cytometer (MoFlo XDPBD, Beckman Coulter, U.S.A).

In vitro cytotoxicity

The cytotoxicity of CM8988-PIPD in comparison with that of its counterparts was evaluated by Cell Counting Kit-8 (CCK-8) and live-dead staining analysis. For CCK-8 analysis, cells were seeded into a 96 well plate at a density of 5×10^4/well and incubated with different concentrations of CM8988-PIPD and counterparts for 48 h. Then, 10 μl CCK-8 (Dojindo Molecular Technologies, Oslo, Norway) was respectively added to each well for another 2 h incubation protected from light. A Multiskan MK3 micro-plate reader (Thermo Fisher Scientific, Massachusetts, USA) was employed to read the absorbance (Ab) at 450 nm to calculate the cell viability of different groups according to the following function:

$$\text{Cell viability\%} = \frac{(Ab_{Samples} - Ab_{Blank})}{(Ab_{Control} - Ab_{Blank})} \times 100\%,$$

where Ab_{blank} are the absorbance values of the culture medium without cells. For live/dead staining, cells were seeded in special culture dishes for CLSM at 2×10^5/dish. Then equal amount of CM8988-PIPD and counterparts were added and co-cultured for 48 h. Cells were then stained with LIVE/DEAD™ Fixable Dead Cell Stain Kits following instructions, and observed by CLSM.

Cellular apoptosis evaluation

Cells were seeded into a 6 well plate at the density of 3×10^5/well and treated with equal amount of CM8988-PIPD and counterparts for 48 h. Then cells were collected, washed with pre-cooled PBS, incubated with Annexin V-Alexa Fluor® 488 and PI in the dark following manufacturer's instructions, and analyzed by a Flow Cytometer. Apoptotic cells were also observed by TEM.

Mitochondrial membrane potentials (MMP) detection

Cells were incubated with equal amount of CM8988-PIPD and counterparts for 48 h. After washing, JC-1 probe (Beyotime Biotechnology, Shanghai China) was employed to measure

mitochondrial depolarization by CLSM following product information.

Western blotting

Cells were collected and suspended in lysis buffer containing protease and phosphatase inhibitors. The protein concentration was quantified by a BCA protein detection kit (Beyotime Biotechnology, Shanghai, China). Equal amount of protein samples was then subjected to SDS-PAGE and immunoblotted with corresponding antibodies (Cell Signaling Technology, Massachusetts, U.S.A.).

Statistical analysis

Statistical analysis was performed by Student's unpaired *t* test or one-way ANOVA to identify significant differences unless otherwise indicated. Differences were considered significant at a *P* value of less than 0.05.

Results and discussion

Characterizations of the PROTAC encapsulated biomimetic DDS

To prepare biomimetic DDS, we firstly extracted the cytomembrane of PATU-8988 cells, and then wrapped PIPD molecules by ultrasound. DLS results reveal that the hydrodynamic size of empty NPs assembled by the cytomembrane of PATU-8988 was approximately 179.3 nm, with a Zeta potential of -9.2 mV. After PIPD encapsulation, the average particle size and Zeta potential has been changed to 124.8 nm and -7.59 mA, respectively (**Figure 2A-C**). TEM results (**Figure 2D**) indicate that the biomimetic NPs possessed a uniform spherical structure, with a diameter of less than 200 nm in accordance with the DLS results. UV/vis (**Figure 2E**) and FTIR (**Figure 2F**) spectra depicted that CM8988-PIPD owns remarkable absorption peaks of both PIPD and empty cytomembrane vesicles, confirming the successful encapsulation of PIPD in cytomembranes. Besides, the retention of membrane ingredients in biomimetic NPs was evaluated by XPS and SDS-PAGE. The XPS results shown in **Figure 2G** demonstrates that CM8988-PIPD contains the same chemical elements as CM8988 cell membrane. And the SDS-PAGE results (**Figure 2H**) shows similar protein composition among CM8988-PIPD, empty cancer cell vesicles (CM8988) and cancer cell lysates.

Excellent serum stability and controlled drug release

It was well expected that our biomimetic DDS could be an excellent drug carrier benefits from the natural and stable structure. Considering the intended use via intravenous administration (I.V.), high serum stability is one of the most important characterizations for an ideal DDS. Therefore, we used the DMEM containing 50% FBS as an *in vitro* serum model to check the serum stability of CM8988-PIPD following previous studies [38, 39]. As we can see from **Figure 3A**, the mean size of CM8988-PIPD experienced no obvious alteration during the experimental period of 6 days, suggesting its excellent serum ability. Also, we found that CM8988-PIPD had a high EE of 65±2.52% for PIPD molecules. **Figure 3B** demonstrates that our biomimetic DDS exhibits a slow drug release in neutral (pH=7.4) environment, with no initial burst during the period of 72 hours. However, the release of PIPD from CM8988 NPs was apparently accelerated at pH 5.0 (mimicking endo/lysosomal environments) with more than 60% PIPDs being released during 24 h. These results indicate that CM8988-PIPD could maintain stability under physiological conditions and release drugs rapidly in the acidic environment of cancer cells, which can avoid premature release of drugs and reduce the side effect to normal tissues.

Favorable in vitro biocompatibility and immunocompatibity

We subsequently investigated the hemocompatibility of the biomimetic DDS by incubation erythrocytes with CM8988-PIPD and counterparts at gradient concentrations. As indicated in **Figure 4A**, free and encapsulated PIPDs all exhibit low hemolysis rate (less than 7%) at different concentrations (from 2.5 to 20 μg/mL). Besides, both free and encapsulated PIPDs demonstrate low-cytotoxicity to human normal pancreatic ductal epithelial cells (HPDE6-C7) in concentrations of up to 32 μg/mL (**Figure 4B**).

It is well established that a variety of artificial nanosized DDSs can be easily recognized and eliminated by the reticuloendothelial system (RES), resulting in shorter circulation time and insufficient accumulation in tumor site [40]. However, studies have shown that cancer cells are able to avoid the recognition of the immune

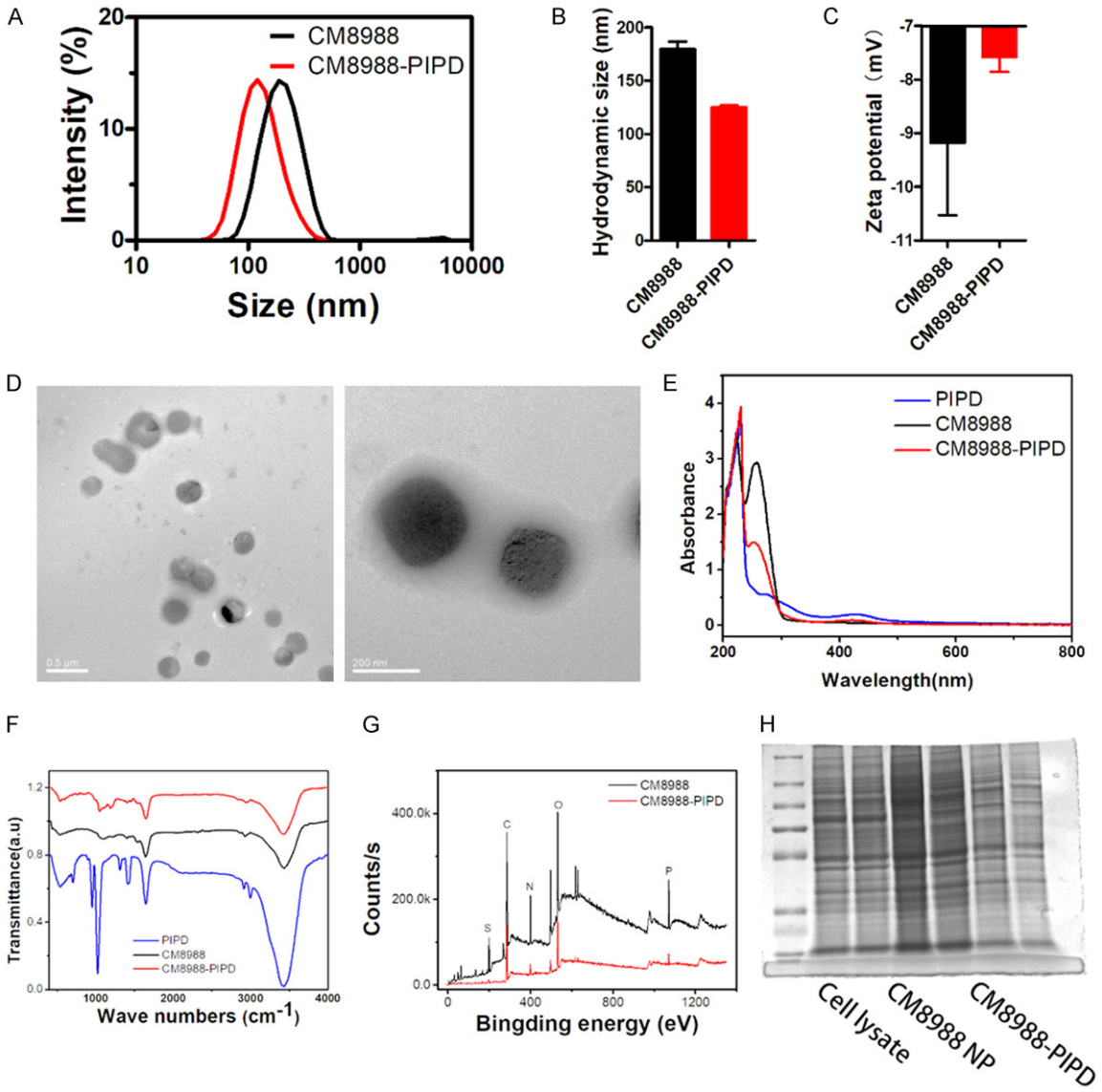

Figure 2. Characterizations of CM8988-PIPD DDS. (A, B) Hydrodynamic size of CM8988-PIPD and empty CM8988 vector by DLS. (C) Surface zeta potential of CM8988-PIPD and empty CM8988 vector. (D) TEM morphology of CM8988-PIPD. Scale bar: left 0.5 μm, right 200 nm. (E-G) UV-vis absorption (E), FTIR spectra (F), and XPS spectrum (G) of CM8988-PIPD and counterparts. (H) SDS-PAGE protein analysis for cell lysates, CM8988 empty ventor and CM8988-PIPD DDS. Data are expressed as mean ± SD (n=3).

system [41, 42], which is employed for particle camouflage in this study. In order to evaluate the immunocompatibility, biomimetic nanoparticles were marked with fluorescence QDs and incubated with J774A.1 macrophages, and the fluorescent QDs swallowed were determined by CLSM. As shown in **Figure 4C**, cytomembrane encapsulated QDs are less prone than free ones to be engulfed by macrophage cells, resulting in weaker green fluorescence in J774A.1 cells, indicating that cancer cell membrane camouflage could effectively inhibited the phagocytosis of macrophages.

Accordingly, all these experimental results demonstrate that our bionic DDS owns favorable biocompatibility and immunocompatibility.

Enhanced cellular uptake by homologous targeting

The cellular uptake of CM8988-PIPD and counterparts was compared in PATU-8988 and PL-45 pancreatic cancer cells. FCM results (**Figure 5A**, **5B**) revealed that encapsulating QDs in the cytomembrane of a nonhomologous

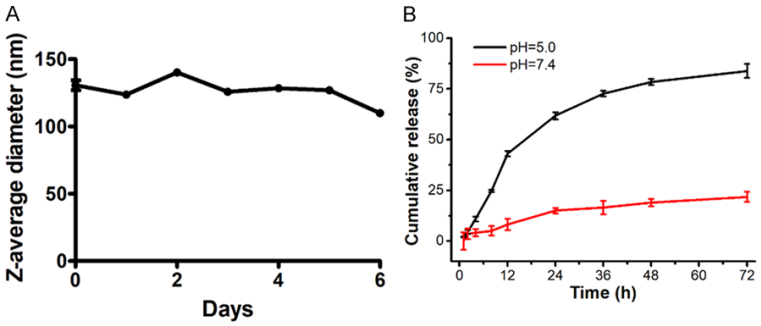

Figure 3. A. Excellent *in vitro* serum stability of CM8988-PIPD nanoparticals: DMEM containing 50% (v/v) FBS was employed as an *in vitro* serum model and the size distribution of CM8988-PIPD was measured by DLS during 6 days. B. Cumulative release of PIPD molecules from CM8988-PIPD DDS at different conditions. Data are expressed as mean ± SD (n=3).

hepatoma cancer cell line (SMMC-7721) can significantly promote the intracellular uptake, indicated by enhanced mean fluorescence intensity (MFI) of both PATU-8988 and PL-45 cells (**P<0.01). On the other hand, cells incubated with homologous cytomembrane encapsulated nanoparticles (CM8988-QDs) showed the highest MFI among all the experimental groups. Similar results were confirmed by CLSM shown in **Figure 5C**, which demonstrates that both cells treated with homologous CM8988-QDs exhibited stronger green fluorescence than cells treated with free QDs and nonhomologous CM7721-QDS. These results indicate that cell membrane coverage can significantly promote endocytosis, and homologous membrane coverage is better than nonhomologous membrane coverage in the promotion.

Excellent in vitro anti-tumor activities

Based on its favorable endocytosis to homologous tumors, the *in vitro* cytotoxicity of CM8988-PIPD and counterparts on both PATU-8988 and PL-45 cells was investigated. As illustrated in **Figure 6A**, **6B**, cells treated with free PIPD experienced a moderate apoptosis rate (indicated by Annexin $V^+/PI^\pm$) of 16.5% and 12.2% for PATU-8988 and PL-45 cells, respectively. Nonhomologous cytomembrane camouflage can remarkably promote PIPD induced cellular apoptosis. Encouragingly, the abovementioned apoptosis inducing activity can be further enhanced by the homologous biomimetic DDS CM8988-PIPD, with a highest apoptosis ratio among groups (PATU-8988 cells: 53.7%, PL-45 cells: 54.3%). Besides, cell apoptosis was confirmed by high resolution transmission electron microscopy, with representative image shown in **Figure 6C**. As we can see, after being treated with different formulations of PIPD, the typical morphologies of apoptotic cells such as chromatic agglutination and formation of apoptotic body could be observed. A CCK-8 test was also employed to evaluate the *in vitro* cytotoxicity of CM8988-PIPD. **Figure 6D**, **6E** demonstrates that for both PC cells, significant higher cytotoxicity of CM8988-PIPD was verified at various drug concentrations than that of CM7721-PIPD and free PIPD (**P<0.01), while CM7721-PIPD showed similar cytotoxicity to that of free PIPD (P>0.05). All these results were validated by live-dead cell staining evaluation, which are based on the reaction of a fluorescent reactive dye with cellular amines. For necrotic cells, the reactive dye can permeate the compromised membranes and react with free amines both in the interior and on the cell surface. In contrast, only the cell-surface amines of viable cells are available to react with the dye, resulting in relatively dim staining. The results in **Figure 6F** further confirmed that homologous targeting significantly enhanced the *in vitro* cytotoxicity of PIPD against PC cells.

We can conclude from the above-mentioned results that our biomimetic DDS owns prominent ability for enhancing the *in vitro* anti-tumor efficacy of containing PROTACs, indicated by increased cellular apoptosis and decreased cell growth. This might be attributed to the co-effects of NP enhanced cellular endocytosis and homologous targeting by PC cell membranes. Besides, the relative acid microenvironment in tumor tissues and cells can significantly promote the accurate PIPD release, which may also participate in the improvement of tumor suppressing activity.

In vitro anti-tumor mechanisms

The satisfactory *in vitro* cytotoxicity of CM8988-PIPD inspired us to evaluate the underlying

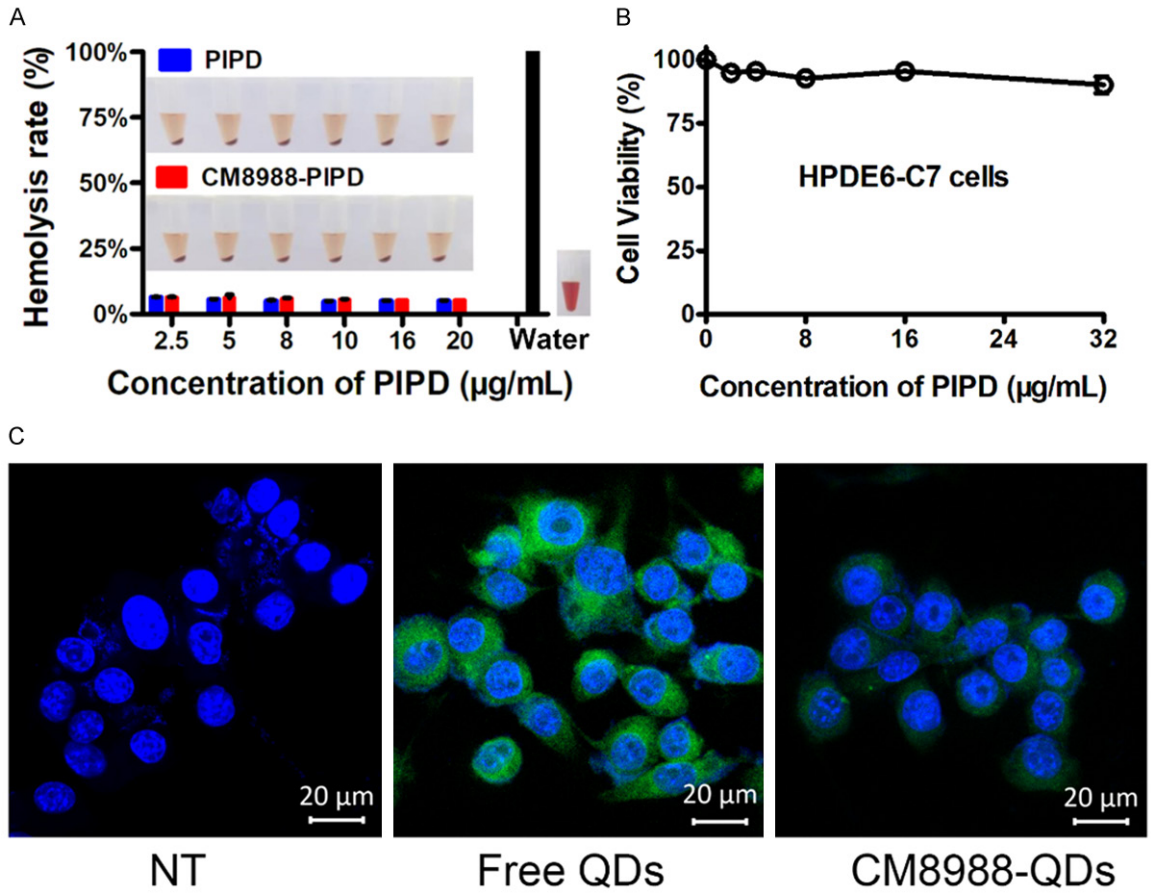

Figure 4. Excellent *in vitro* biocompatibility and immunocompatibility of biomimetic DDS. A. Hemolysis rate of red blood cells in different concentrations of free and CM8988 encapsulated PIPDs. B. The cell viability of human normal pancreatic ductal epithelial cells (HPDE6-C7) treated with different concentrations of CM8988-PIPD. C. CLSM images of J774A.1 macrophages co-culture with free and CM8988 encapsulated QDs for 4 h. Green and blue fluorescence indicates QD and nucleus, respectively. Scale bar: 20 μm.

antitumor mechanisms. Mitochondrial depolarization is a feature of cell apoptosis. In normal cells, the mitochondrial membrane potential is higher and JC-1 gathers in the matrix of mitochondria to form a polymer to produce red fluorescence. Conversely, the mitochondrial membrane potential decreases during apoptosis to produce green fluorescence. In order to determine the alteration of mitochondrial membrane potential, we firstly detected mitochondrial depolarization in targeting cells by CLSM post JC-1 staining. As shown in **Figure 7A**, the mitochondrial depolarization in CM7721-PIPD treated group was higher than that in PIPD and control groups, being indicated by a decreased fluorescence in JC-1 red and an increased fluorescence in JC-1 green. At the same condition, the mitochondrial depolarization appeared in homologous DDS (CM8988-PIPD) treated group was remarkably higher than that in nonhomologous DDS (CM7721-PIPD) treated group. The activation of Caspase 9, which pays vital roles in cellular apoptosis, shows similar trends as mitochondrial depolarization (**Figure 7C**).

Subsequently, PDEδ degradation was tested in both PC cells. The degradative potency for PDEδ was firstly evaluated in PATU-8988 cells according to WB analysis. As illustrated in **Figure 7B**, free and CM8988 encapsulated PIPD can efficiently induce PDEδ degradation in both concentration and time dependent manners. Moreover, CM8988 encapsulated PIPD than free PIPD exhibited stronger PDEδ degrading ability in tested concentrations and periods. **Figure 7C** demonstrates that CM8988-PIPD shows distinguished PDEδ

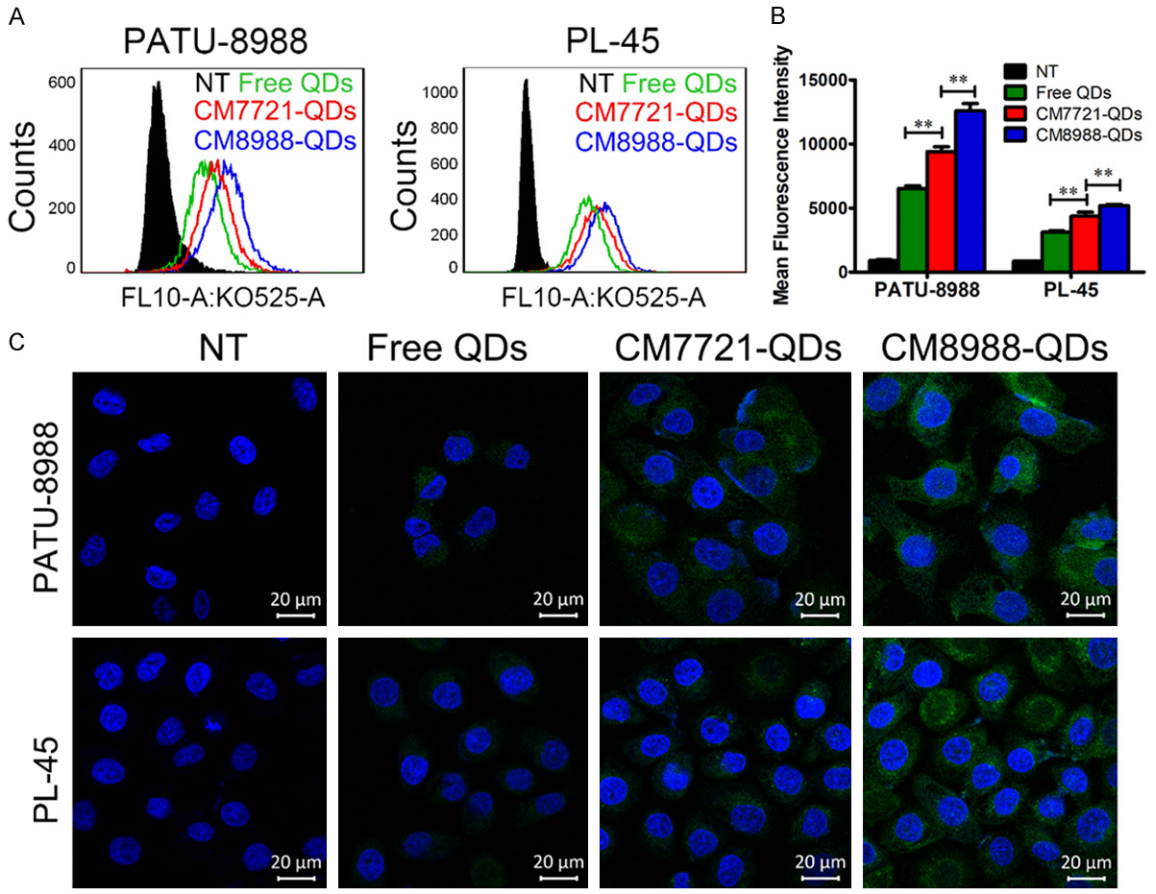

Figure 5. Assessment of cellular uptake of biomimetic DDS by FCM and CLSM. A. Effects of cytomembrane on the intracellular uptake of QDs by homologous malignant pancreatic cells (PATU-8988 and PL-45) by FCM. B. Quantitative analysis of FCM results. Mean fluorescence intensity was counted using FlowJo software. Data are mean ± SD (n=3), $^{**}P<0.01$. C. CLSM images of PATU-8988 and PL-45 cells co-culture with free and cytomembrane encapsulated QDs. Green and blue fluorescence indicates QD and nucleus, respectively. Scale bar: 20 μm.

degrading ability when compared with free and CM7721 encapsulated PIPDs in both PATU-8988 and PL-45 cells.

RAS proteins regulate PI3K-AKT and Raf-MEK1/2 signal transduction pathways associated with cell proliferation, apoptosis, and differentiation [43]. For further investigating the impact of CM8988-PIPD, we evaluated the phosphorylation of AKT and extracellular signal regulated kinase (Erk), which play pivotal roles in PI3K-AKT and Raf-MEK1/2 signaling. WB results (**Figure 7C**) indicate that free and CM7721 encapsulated PIPDs effectively reduced AKT and Erk phosphorylation in both PATU-8988 and PL-45 cells. In contrast, homologous CM8988-PIPD owns the most prominent efficacy for downregulating both p-AKT and p-Erk. All these results confirmed that CM8988-PIPD is a splendid PDEδ degrader, which can significantly induce cellular apoptosis and proliferation suppression via the inhibition of RAS signaling.

Conclusions

In this study, a prominent nano-drug delivery system was successfully constructed by biomimetic strategy for targeted delivery of a first-in-class PDEδ degrader, PIPD, which was identified by PROTAC approach in our previous study [20]. PATU-8988 cytomembrane camouflage endowed the biomimetic DDS (CM8988-PIPD) with excellent *in vitro* serum stability, ideal controlled drug release profile, favorable biocompatibility & immunocompatibility, and prominent targeting ability to homologous tumors. Owing to these advantages, the smart DDS sig-

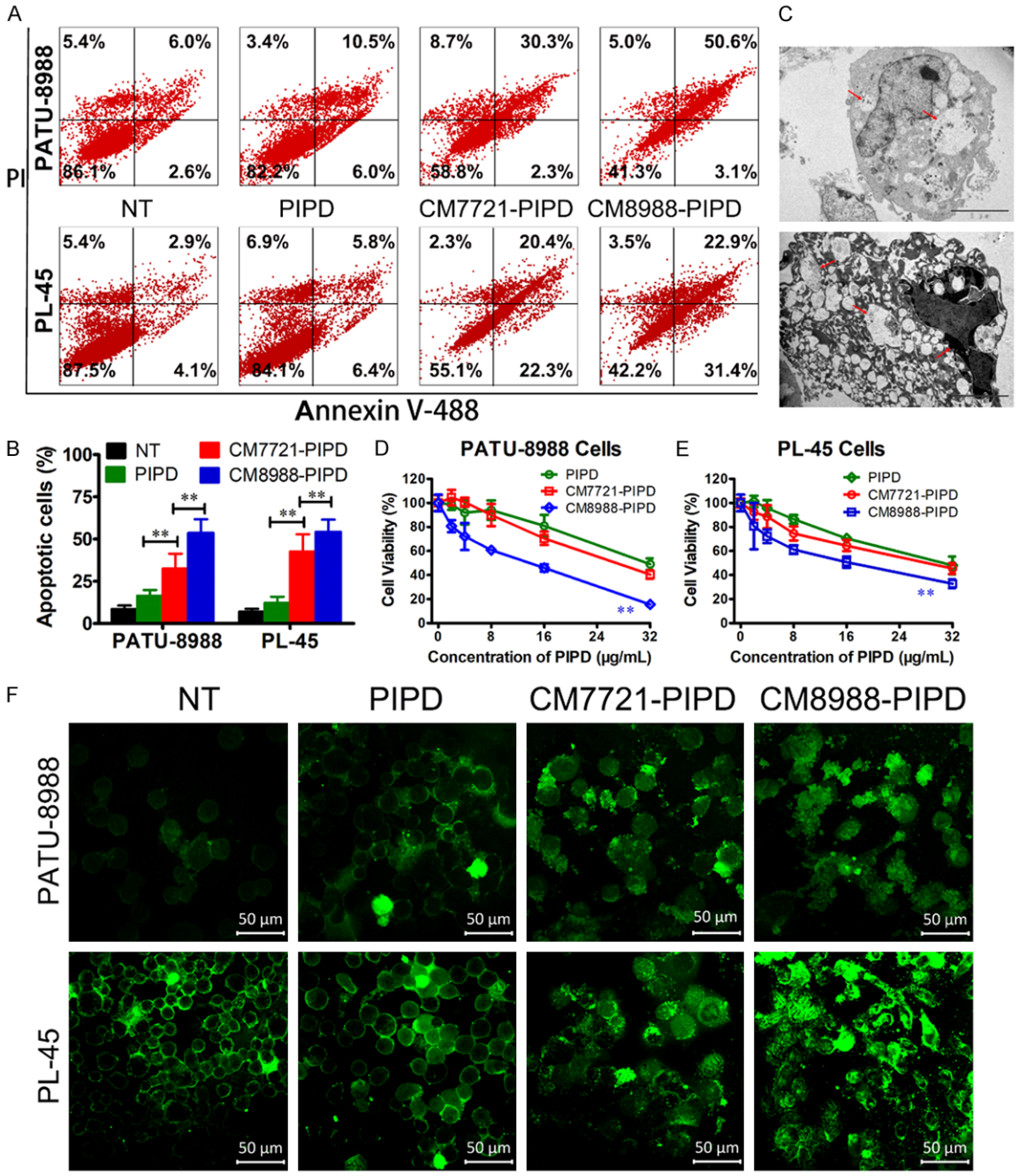

Figure 6. *In vitro* cytotoxicity evaluation of biomimetic DDS. (A) Cellular apoptosis of PATU-8988 and PL-45 cells treated with CM8988-PIPD and counterparts by FCM. (B) Quantitative analysis of FCM results. Apoptotic cells were defined as Annexin $V^+/PI^\pm$ cells. (C) Bio-TEM images of apoptotic PATU-8988 (up panel) and PL-45 (down panel) cells. The red arrows indicated typical morphologies of apoptosis including chromatic agglutination and formation of apoptotic body. Cell viability of (D) PATU-8988 and (E) PL-45 cells after treatment with different concentrations of free and encapsulated PIPD by CCK-8 analysis. (F) Live/dead staining of PATU-8988 and PL-45 cells with different treatments. For necrotic cells, the reactive dye can permeate the compromised membranes and react with free amines both in the interior and on the cell surface. In contrast, only the cell-surface amines of viable cells are available to react with the dye, resulting in relatively dim staining. Scale bar: 50 μm. All the data are mean ± SD (n=3), $^{**}P<0.01$.

nificantly enhanced the PDEδ degrading efficacy, remarkably inducing cellular apoptosis and proliferation suppression via the inhibition of RAS signaling. *In vitro* studies illustrated that

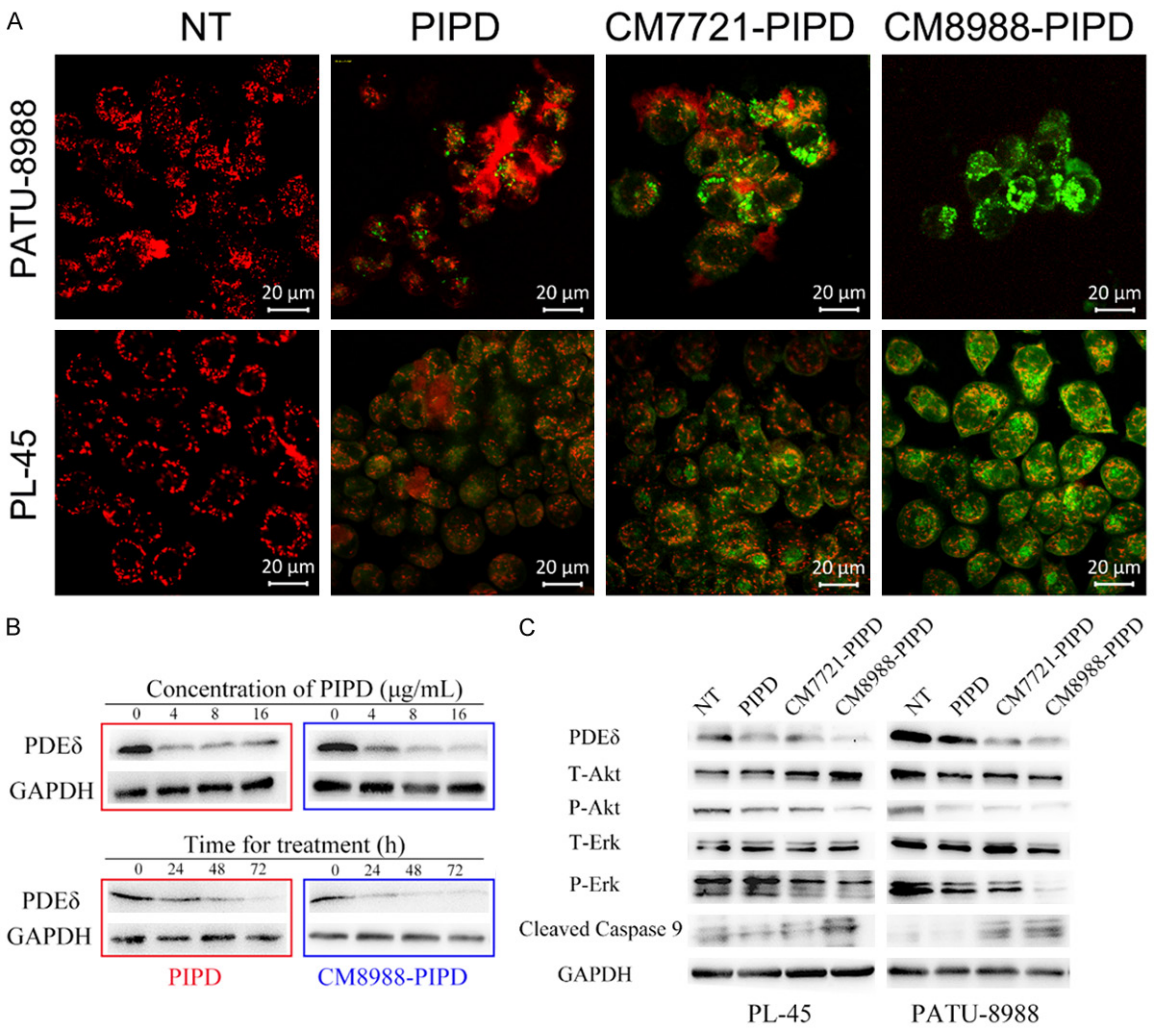

Figure 7. A. Changes in mitochondrial membrane potential of PATU-8988 and PL-45 cells treated with free and encapsulated PIPD by CLSM. Scale bar: 20 μm. B. Relative protein expression of PDEδ in PATU-8988 cells after treated with different concentrations of PIPD and CM8988-PIPD for different times by WB. C. Relative protein expression of PDEδ, T-AKT, P-AKT, T-Erk, P-Erk, and Cleaved Caspase 9 in PATU-8988 and PL-45 cells treated with different formulations of PIPD.

CM8988-PIPD is more effective than free and nonhomologous CM7721 encapsulated PIPDs in killing both tested PC cells. In conclusion, the versatile biomimetic DDS CM8988-PIPD hold great potential for the treatment of homologous pancreatic carcinoma, with which we expect to augment the therapeutic efficiency and minimize undesired side effects of PROTAC molecules by mimicking or directly taking advantage of the ways that cells interact and communicate with living entities. The biomimetic designs fuse "life" to NPs and enable them to "communicate" with cancer cells and cancer microenvironment [44]. It is worth mentioning that the biomimetic strategy is not independent and can be combined with bionanotechnologies, bioconjugation chemistry, pharmaceutical chemistry, and biomedical engineering together to develop more potent formulations in both pre-clinical and clinical studies in the future [44, 45]. However, there are still serious challenges that need to be overcome in this field. For instance, although the viability and desired biological functions of biomimetic NPs could be well preserved, the undesired effects on their other functions and long-term behaviors in biological systems should be thoroughly assessed [44]. Besides, for biological membrane-derived biomimetic nanomedicines, concerns regarding reproducibility of the quan-

tities of membrane proteins, and their scale-up manufacturing have to be addressed [44, 45]. In addition, everything will need to be carried out aseptically and done in a manner that complies with good manufacturing processes, ensuring that the final products are free from both chemical and biological contaminants [46]. As this emerging biomimetic technology begins to mature, attempts will be made to translate such platforms from bench to beside, where they are primed to make positive impacts on human health.

Acknowledgements

This work was granted by "One Belt One Road" International Cooperation Project of Shanghai Municipal Committee of Science and Technology (Grant No. 19410740900) and the Natural Science Foundation of Shanghai (Grant No. 21ZR1422800, 19ZR1442900).

Disclosure of conflict of interest

None.

Address correspondence to: Dr. Huafei Li, School of Lifesciences, Shanghai University, 333 Nanchen Road, Shanghai 200444, China. E-mail: huafey_lee@163.com; Dr. Guoqiang Dong, Department of Medicinal Chemistry, School of Pharmacy, Second Military Medical University, 325 Guohe Road, Shanghai 200433, China. E-mail: gdong@smmu.edu.cn

References

[1] Pereira SP, Oldfield L, Ney A, Hart PA, Keane MG, Pandol SJ, Li D, Greenhalf W, Jeon CY, Koay EJ, Almario CV, Halloran C, Lennon AM and Costello E. Early detection of pancreatic cancer. Lancet Gastroenterol Hepatol 2020; 5: 698-710.

[2] Sung H, Ferlay J, Siegel RL, Laversanne M, Soerjomataram I, Jemal A and Bray F. Global cancer statistics 2020: GLOBOCAN estimates of incidence and mortality worldwide for 36 cancers in 185 countries. CA Cancer J Clin 2021; 71: 209-249.

[3] Siegel RL, Miller KD, Fuchs HE and Jemal A. Cancer statistics, 2022. CA Cancer J Clin 2022; 72: 7-33.

[4] Neoptolemos JP, Kleeff J, Michl P, Costello E, Greenhalf W and Palmer DH. Therapeutic developments in pancreatic cancer: current and future perspectives. Nat Rev Gastroenterol Hepatol 2018; 15: 333-348.

[5] Owens DK, Davidson KW, Krist AH, Barry MJ, Cabana M, Caughey AB, Curry SJ, Doubeni CA, Epling JJ, Kubik M, Landefeld CS, Mangione CM, Pbert L, Silverstein M, Simon MA, Tseng CW and Wong JB. Screening for pancreatic cancer: US preventive services task force reaffirmation recommendation statement. JAMA 2019; 322: 438-444.

[6] Ferguson FM and Gray NS. Kinase inhibitors: the road ahead. Nat Rev Drug Discov 2018; 17: 353-377.

[7] Rajewsky K. The advent and rise of monoclonal antibodies. Nature 2019; 575: 47-49.

[8] Topalian SL, Taube JM and Pardoll DM. Neoadjuvant checkpoint blockade for cancer immunotherapy. Science 2020; 367: eaax0182.

[9] Liu J, Ma J, Liu Y, Xia J, Li Y, Wang ZP and Wei W. PROTACs: a novel strategy for cancer therapy. Semin Cancer Biol 2020; 67: 171-179.

[10] Liu XJ, Xu-Liu, Pang XJ, Ying YX, Yu GX, Li YR, Guan YF, Zhang YB, Song J, Zhang QR and Zhang SY. Progress in the development of small molecular inhibitors of the Bruton's tyrosine kinase (BTK) as a promising cancer therapy. Bioorg Med Chem 2021; 47: 116358.

[11] O'Bryan JP. Pharmacological targeting of RAS: recent success with direct inhibitors. Pharmacol Res 2019; 139: 503-511.

[12] Downward J. Targeting RAS signalling pathways in cancer therapy. Nat Rev Cancer 2003; 3: 11-22.

[13] Gillson J, Ramaswamy Y, Singh G, Gorfe AA, Pavlakis N, Samra J, Mittal A and Sahni S. Small molecule KRAS inhibitors: the future for targeted pancreatic cancer therapy? Cancers (Basel) 2020; 12: 1341.

[14] Roskoski RJ Jr. Blockade of mutant RAS oncogenic signaling with a special emphasis on KRAS. Pharmacol Res 2021; 172: 105806.

[15] Morris JT, Wang SC and Hebrok M. KRAS, Hedgehog, Wnt and the twisted developmental biology of pancreatic ductal adenocarcinoma. Nat Rev Cancer 2010; 10: 683-695.

[16] Buscail L, Bournet B and Cordelier P. Role of oncogenic KRAS in the diagnosis, prognosis and treatment of pancreatic cancer. Nat Rev Gastroenterol Hepatol 2020; 17: 153-168.

[17] Indini A, Rijavec E, Ghidini M, Cortellini A and Grossi F. Targeting KRAS in solid tumors: current challenges and future opportunities of novel KRAS inhibitors. Pharmaceutics 2021; 13: 653.

[18] Ozdemir ES, Jang H, Gursoy A, Keskin O and Nussinov R. Arl2-mediated allosteric release of farnesylated kras4b from shuttling factor PDEdelta. J Phys Chem B 2018; 122: 7503-7513.

[19] Schmick M, Kraemer A and Bastiaens PI. Ras moves to stay in place. Trends Cell Biol 2015; 25: 190-197.

[20] Cheng J, Li Y, Wang X, Dong G and Sheng C. Discovery of novel PDEdelta degraders for the treatment of kras mutant colorectal cancer. J Med Chem 2020; 63: 7892-7905.
[21] Salami J and Crews CM. Waste disposal-an attractive strategy for cancer therapy. Science 2017; 355: 1163-1167.
[22] Zou Y, Ma D and Wang Y. The PROTAC technology in drug development. Cell Biochem Funct 2019; 37: 21-30.
[23] Dale B, Cheng M, Park KS, Kaniskan HU, Xiong Y and Jin J. Advancing targeted protein degradation for cancer therapy. Nat Rev Cancer 2021; 21: 638-654.
[24] Burslem GM and Crews CM. Proteolysis-targeting chimeras as therapeutics and tools for biological discovery. Cell 2020; 181: 102-114.
[25] Churcher I. Protac-induced protein degradation in drug discovery: breaking the rules or just making new ones? J Med Chem 2018; 61: 444-452.
[26] Saenz DT, Fiskus W, Qian Y, Manshouri T, Rajapakshe K, Raina K, Coleman KG, Crew AP, Shen A, Mill CP, Sun B, Qiu P, Kadia TM, Pemmaraju N, DiNardo C, Kim MS, Nowak AJ, Coarfa C, Crews CM, Verstovsek S and Bhalla KN. Novel BET protein proteolysis-targeting chimera exerts superior lethal activity than bromodomain inhibitor (BETi) against post-myeloproliferative neoplasm secondary (s) AML cells. Leukemia 2017; 31: 1951-1961.
[27] Hu CM, Fang RH, Wang KC, Luk BT, Thamphiwatana S, Dehaini D, Nguyen P, Angsantikul P, Wen CH, Kroll AV, Carpenter C, Ramesh M, Qu V, Patel SH, Zhu J, Shi W, Hofman FM, Chen TC, Gao W, Zhang K, Chien S and Zhang L. Nanoparticle biointerfacing by platelet membrane cloaking. Nature 2015; 526: 118-121.
[28] Wang C, Zhang W, He Y, Gao Z, Liu L, Yu S, Hu Y, Wang S, Zhao C, Li H, Shi J, Zhou W, Li F, Yue H, Li Y, Wei W, Ma G and Ma D. Ferritin-based targeted delivery of arsenic to diverse leukaemia types confers strong anti-leukaemia therapeutic effects. Nat Nanotechnol 2021; 16: 1413-1423.
[29] Xue G, Zhang Y, Xie T, Zhang Z, Liu Q, Li X and Gou X. Cell adhesion-mediated piezoelectric self-stimulation on polydopamine-modified poly(vinylidene fluoride) membranes. ACS Appl Mater Interfaces 2021; 13: 17361-17371.
[30] Chai Z, Ran D, Lu L, Zhan C, Ruan H, Hu X, Xie C, Jiang K, Li J, Zhou J, Wang J, Zhang Y, Fang RH, Zhang L and Lu W. Ligand-modified cell membrane enables the targeted delivery of drug nanocrystals to glioma. Acs Nano 2019; 13: 5591-5601.
[31] Li H, Jin H, Wan W, Wu C and Wei L. Cancer nanomedicine: mechanisms, obstacles and strategies. Nanomedicine (Lond) 2018; 13: 1639-1656.
[32] Liu L, Bai X, Martikainen MV, Karlund A, Roponen M, Xu W, Hu G, Tasciotti E and Lehto VP. Cell membrane coating integrity affects the internalization mechanism of biomimetic nanoparticles. Nat Commun 2021; 12: 5726.
[33] Liu W, Ruan M, Wang Y, Song R, Ji X, Xu J, Dai J and Xue W. Light-triggered biomimetic nanoerythrocyte for tumor-targeted lung metastatic combination therapy of malignant melanoma. Small 2018; 14: e1801754.
[34] Jin J, Krishnamachary B, Barnett JD, Chatterjee S, Chang D, Mironchik Y, Wildes F, Jaffee EM, Nimmagadda S and Bhujwalla ZM. Human cancer cell membrane-coated biomimetic nanoparticles reduce fibroblast-mediated invasion and metastasis and induce T-cells. ACS Appl Mater Interfaces 2019; 11: 7850-7861.
[35] Jin J and Bhujwalla ZM. Biomimetic nanoparticles camouflaged in cancer cell membranes and their applications in cancer theranostics. Front Oncol 2019; 9: 1560.
[36] Kroll AV, Fang RH, Jiang Y, Zhou J, Wei X, Yu CL, Gao J, Luk BT, Dehaini D, Gao W and Zhang L. Nanoparticulate delivery of cancer cell membrane elicits multiantigenic antitumor immunity. Adv Mater 2017; 29: 10.1002/adma.201703969.
[37] Kim I, Lee D, Lee SW, Lee JH, Lee G and Yoon DS. Coagulation-inspired direct fibrinogen assay using plasmonic nanoparticles functionalized with red blood cell membranes. Acs Nano 2021; 15: 6386-6394.
[38] Mussi SV, Sawant R, Perche F, Oliveira MC, Azevedo RB, Ferreira LA and Torchilin VP. Novel nanostructured lipid carrier co-loaded with doxorubicin and docosahexaenoic acid demonstrates enhanced in vitro activity and overcomes drug resistance in MCF-7/Adr cells. Pharm Res 2014; 31: 1882-1892.
[39] Li H, Guo K, Wu C, Shu L, Guo S, Hou J, Zhao N, Wei L, Man X and Zhang L. Controlled and targeted drug delivery by a uv-responsive liposome for overcoming chemo-resistance in nonhodgkin lymphoma. Chem Biol Drug Des 2015; 86: 783-794.
[40] Chen G, Yang Y, Xu Q, Ling M, Lin H, Ma W, Sun R, Xu Y, Liu X, Li N, Yu Z and Yu M. Self-amplification of tumor oxidative stress with degradable metallic complexes for synergistic cascade tumor therapy. Nano Lett 2020; 20: 8141-8150.
[41] Jin F, Qi J, Liu D, You Y, Shu G, Du Y, Wang J, Xu X, Ying X, Ji J and Du Y. Cancer-cell-biomimetic Upconversion nanoparticles combining chemo-photodynamic therapy and CD73 blockade for metastatic triple-negative breast cancer. J Control Release 2021; 337: 90-104.
[42] Qu Y, Chu B, Wei X, Chen Y, Yang Y, Hu D, Huang J, Wang F, Chen M, Zheng Y and Qian Z. Can-

cer-cell-biomimetic nanoparticles for targeted therapy of multiple myeloma based on bone marrow homing. Adv Mater 2021: e2107883.
[43] Zimmermann G, Papke B, Ismail S, Vartak N, Chandra A, Hoffmann M, Hahn SA, Triola G, Wittinghofer A, Bastiaens PI and Waldmann H. Small molecule inhibition of the KRAS-PDEdelta interaction impairs oncogenic KRAS signalling. Nature 2013; 497: 638-642.
[44] Chen Z, Wang Z and Gu Z. Bioinspired and biomimetic nanomedicines. Acc Chem Res 2019; 52: 1255-1264.
[45] van der Meel R, Sulheim E, Shi Y, Kiessling F, Mulder W and Lammers T. Smart cancer nanomedicine. Nat Nanotechnol 2019; 14: 1007-1017.
[46] Fang RH, Kroll AV, Gao W and Zhang L. Cell membrane coating nanotechnology. Adv Mater 2018; 30: e1706759.